JOURNAL OF GUIDANCE, CONTROL, AND DYNAMICS
Vol. 25, No. 3, May–June 2002

Two-Degree-of-Freedom Control of an Actively Controlled Wind-Tunnel Model

George Papageorgiou* and Keith Glover†
University of Cambridge, Cambridge, England CB2 1PZ, United Kingdom

A robust two-degree-of-freedom controller is designed for an actively controlled wind-tunnel model. The wind-tunnel model is geometrically similar to the High Incidence Research Model that was used in the design challenge set up by the Group for Aeronautical Research and Technology in Europe. The design procedure with which the two-degree-of-freedom controller is designed is based on standard two-degree-of-freedom $\mathcal{H}_\infty$ loop shaping. This design procedure enables the designer to meet time-domain specifications, defined with respect to the transfer matrix from references to controlled outputs (or a subset of the controlled outputs), accurately and robustly, subject to a robust stability constraint. The controller is flight tested and very satisfactory performance is achieved.

I. Introduction

TWO-DEGREE-OF-FREEDOM control arises from disturbance rejection being entirely decoupled from nominal tracking (for example, see Ref. 1). Therefore, the control system designer can use one degree of freedom (DOF) to meet the disturbance rejection (and/or robust stability) requirements and the other DOF to meet the nominal tracking requirements. The design of two-DOF (2-DOF) controllers has received a lot of attention in the control literature, for example, see Refs. 1–5 and references therein.

In flight control, robust tracking of the pilot's commands is very important. Designing 2-DOF controllers that meet robust tracking specifications has been the subject of many papers, for example, see Refs. 3, 4, and 6. The design procedure detailed in Ref. 3 and referred to hereafter as standard 2-DOF $\mathcal{H}_\infty$ loop shaping has been used to design flight control laws for the Westland Lynx multirole combat helicopter and the National Research Council of Canada's Bell 205 airborne simulator. Both control laws were tested thoroughly, the former in ground-based simulation and the later in flight, and both performed very well.[7,8]

Many $\mathcal{H}_\infty$-based 2-DOF controller design methods employ an ideal reference model to enforce nominal and robust tracking requirements, for example, see Refs. 3 and 6. An alternative method that does not use an ideal reference model is presented in Ref. 9.

The aim of this paper is to design a robust 2-DOF controller for the High Incidence Research Model (HIRM) wind-tunnel model.[10] The procedure used to design the 2-DOF controller enables the designer to design systematically controllers that meet time-domain specifications, defined with respect to the transfer matrix from references to controlled outputs, accurately and robustly subject to a robust stability constraint. This design procedure is based on the standard 2-DOF $\mathcal{H}_\infty$ loop shaping setup, but the optimization problem solved for controller synthesis is new: 1) The structure of the problem is exploited by using μ-synthesis techniques. 2) A robust stability constraint is included in the optimization.

Before proceeding, $\mathcal{H}_\infty$ loop shaping will be reviewed. The $\mathcal{H}_\infty$ loop shaping design procedure, which was proposed by McFarlane and Glover,[11] is a very sensible and appealing procedure for designing robust controllers.[12] It is a combination of loop shaping[13] and robust stabilization and is described hereafter:

1) Shape the singular values of G open loop with frequency-dependent weights W_1 and W_2 according to closed-loop objectives. [G denotes a linear time-invariant (LTI) model of the plant for which the controller is designed.] The weighted plant $G_s = W_2 G W_1 = \tilde{M}^{-1}\tilde{N}$, where $\{\tilde{M}, \tilde{N}\}$ is a normalized left coprime factorization (LCF) of G_s, is depicted in Fig. 1.

2) Minimize the $\mathcal{H}_\infty$ norm of the transfer matrix from disturbances w_1 and w_2 to errors z_1 and z_2 over all stabilizing controllers K_∞, that is,

$$\min_{\text{stab } K_\infty} \left\| \begin{bmatrix} w_1 \\ w_2 \end{bmatrix} \to \begin{bmatrix} z_1 \\ z_2 \end{bmatrix} \right\|_\infty = \gamma_{\text{RS}}$$

Check the achieved γ_{RS}; γ_{RS} is a measure of how robust the desired loop shape G_s is to perturbations $\Delta_{\tilde{M}}, \Delta_{\tilde{N}} \in \mathcal{RL}_\infty$ of its normalized coprime factors $\tilde{M}$ and $\tilde{N}$. (The space $\mathcal{RL}_\infty$ consists of all proper and real rational transfer matrices with no poles on the imaginary axis.) Note that $\Delta_{\tilde{M}}$ and $\Delta_{\tilde{N}}$ can be regarded as low- and high-frequency loop perturbations, respectively. (By the term loop perturbations, it is meant perturbations to the output and input loop transfer matrices defined as $GW_1K_\infty W_2$ and $W_1K_\infty W_2G$, respectively.)

3) Choose the position of K_∞ in the loop. Model reduce the controller and design the command prefilters.

4) Check time simulations and frequency responses of the resulting closed-loop system to verify robust performance. Iterations may be required.

The theoretical basis for $\mathcal{H}_\infty$ loop shaping is that K_∞ does not modify the desired loop shape G_s significantly at low and high frequencies if γ_{RS} is not too large.[11] Therefore, the designer can define performance objectives by shaping the open-loop model G with weights W_1 and W_2.

The synthesized controller K_∞ can be implemented in three ways: in the forward path, in the feedback path, and in the observer form. (For details about how to implement K_∞ as an exact observer of G_s with state feedback see Appendix A.3 of Ref. 14.) The block diagrams of the closed loops that result from implementing K_∞ in the forward path, the feedback path, and in the observer form can be redrawn as shown in Fig. 2. The block K in Fig. 2 can be partitioned as $K = [\hat{K} \;\; K_\infty]$; thus, if, for example, K_∞ is implemented in the forward path, then $\hat{K} = K_\infty W_2$.

When designing a controller with $\mathcal{H}_\infty$ loop shaping, the designer cannot always shape $T_{r\to y}$ accurately and robustly according to time-domain specifications defined with respect to $T_{r\to y}$. ($T_{r\to y}$ is the transfer matrix from references r to controlled outputs y; see Fig. 2.) Assume that the controller will be implemented in the forward path, that is, $T_{r\to y} = (I - L_o)^{-1}L_o$. ($L_o = GW_1K_\infty W_2$ is the output loop transfer matrix.) It can be difficult to translate the time response requirements defined with respect to $T_{r\to y}$ into frequency-domain specifications for L_o. This difficulty arises because it is not

Presented as Paper 99-4274 at the AIAA 17th Applied Aerodynamics Conference, Norfolk, VA, 28 June–1 July 1999; received 8 October 2000; revision received 5 November 2001; accepted for publication 10 November 2001.

*Research Associate, Department of Engineering; currently Postdoctoral Researcher, Department of Aerospace Engineering and Mechanics, University of Minnesota, Minneapolis, Minnesota 55455. Member AIAA.
†Professor, Department of Engineering.

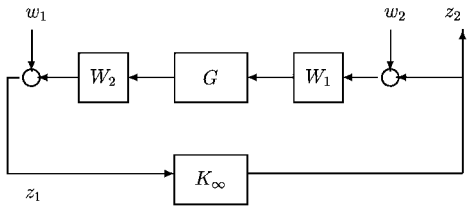

Fig. 1 $\mathcal{H}_\infty$ loop shaping standard block diagram.

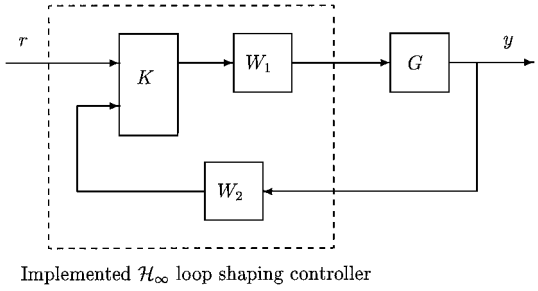

Fig. 2 Implemented closed-loop system.

always clear how the individual transfer functions of L_o affect $T_{r\to y}$. Even if it is, it is not straightforward to shape the individual transfer functions of L_o with the weights W_1 and W_2. To add to this, the weighted plant will be modified to some extent by the synthesised controller K_∞, though if $\gamma_{\rm RS}$ and $\kappa(W_2)$ are not too large [where $\kappa(W_2)$ denotes the condition number of W_2], then L_o will be close to the weighted plant.[11] Furthermore, it is hard to shape L_o so that in the presence of loop perturbations nominal tracking degrades as desired. Similar difficulties arise when K_∞ is implemented in the feedback path or in the observer form.

The preceding discussion motivates the need for a design procedure that retains the appealing features of $\mathcal{H}_\infty$ loop shaping and enables the designer to design systematically controllers that 1) meet time-response requirements defined with respect to $T_{r\to y}$ accurately, 2) maintain such requirements to a certain extent in the presence of loop perturbations, and 3) guarantee some prespecified level of robust stability with respect to loop perturbations. Many flight controller specifications fall into one of these three categories, for example, single- and multi-loop gain and phase margins fall into category 3 (Ref. 15).

What follows is a brief outline of the paper. Section II formalizes and comments on the guarantees that the 2-DOF controller must provide. In Sec. III, the $\mathcal{H}_\infty$ loop shaping setup is modified, and the optimization problem used for controller synthesis is motivated. Section IV deals with solving the optimization problem, and Secs. V and VI detail and comment on the design procedure. Finally, Secs. VII and VIII describe the HIRM wind-tunnel model, controller design, and flight-testing results.

The notation employed throughout this paper is standard.

II. Guarantees That the 2-DOF Controller Must Provide

Assume that the 2-DOF controller is made up of three components as illustrated in Fig. 2, and that the model of the plant for which the controller is designed is denoted by G. The guarantees about the closed-loop system that the 2-DOF controller must provide are the following:

1) The 2-DOF controller must provide robust stability (RS) with respect to uncertainty in the normalized coprime factors of the weighted plant $G_s = W_2 G W_1$:

$$\|[\Delta_{\tilde M} \quad \Delta_{\tilde N}]\|_\infty \le \gamma_{\rm RS}^{-1}$$

where $\gamma_{\rm RS}^{-1}$ is the stability margin.

2) The 2-DOF controller must provide nominal performance (NP) with respect to an ideal reference model T_0:

$$\|T_{r\to y} - T_0\|_\infty < \delta_{\rm NP}$$

where $\delta_{\rm NP}$ is the NP level.

3) The 2-DOF controller must provide robust performance (RP) with respect to an ideal reference model T_0:

$$\|\hat T_{r\to y} - T_0\|_\infty < \delta_{\rm RP} \qquad \forall \|[\Delta_{\tilde M} \quad \Delta_{\tilde N}]\|_\infty \le \gamma_{\rm RP}^{-1}$$

where $\hat T_{r\to y}$ is the perturbed transfer matrix from references to outputs (perturbed due to perturbations in the normalized coprime factors of the weighted plant), $\delta_{\rm RP}$ is the RP level, and $\gamma_{\rm RP}^{-1}$ is the performance margin.

A design procedure that enables the designer to synthesize a controller that comes with the preceding guarantees is only of use if the designer can choose $\gamma_{\rm RS}$, T_0, $\delta_{\rm NP}$, $\delta_{\rm RP}$, and $\gamma_{\rm RP}$ in a meaningful manner. In the rest of this section, a number of observations will be made about $\gamma_{\rm RS}$, T_0, $\delta_{\rm NP}$, $\delta_{\rm RP}$, and $\gamma_{\rm RP}$ that will demonstrate that they can be chosen in a meaningful manner.

The stability margin $\gamma_{\rm RS}^{-1}$ summarizes a lot of information about the closed-loop system. Some types of RP and single- and multi-loop Nichols plot tests can all be related to the stability margin.[12,15] Engineering experience indicates that if the value of $\gamma_{\rm RS}^{-1}$ is greater than 0.2, then the closed-loop system will be robust and behave as specified.[8,10,16]

It is easy to translate the time response specifications of each channel of $T_{r\to y}$ into the frequency domain, that is, into a transfer function T_0^i, $i = 1, \ldots, p$, where p is the number of controlled outputs. This results in a diagonal transfer matrix, $\mathrm{diag}(T_0^1, \ldots, T_0^p)$, which is called the ideal reference model and is denoted by T_0. That T_0 is diagonal emphasizes output decoupling. In the case of military aircraft, the time-response specifications of each closed-loop channel are provided by the MIL-STD. An alternative approach for designing T_0 would be to design a controller with a performance-oriented method, such as nonlinear dynamic inversion or eigenstructure assignment, and to use the resulting transfer matrix from references to outputs as the ideal reference model.

The designer usually has a feel for the type and size of the uncertainty associated with the nominal plant model. For example, the nominal HIRM models used in the Group for Aeronautical Research and Technology in Europe (GARTEUR) design challenge[17] were supplied with a set of plausible perturbed models. A ν-gap analysis can provide a sensible measure of the desired performance margin ($\gamma_{\rm RP}^{-1}$). Thus,

$$\gamma_{\rm RP}^{-1} = \max_i \delta_\nu(W_2 \hat G_i W_1, W_2 G W_1)$$

where $\hat G_i$ are the perturbed plant models. For a definition and discussion of the ν-gap metric, see Refs. 14 and 18.

The guarantee

$$\|\hat T_{r\to y} - T_0\|_\infty < \delta_{\rm RP}$$

can be used to provide estimates of the step response properties of $\hat T_{r\to y}$ (rise time, settling time, and overshoot) if the RP level is smaller than one, that is, $\delta_{\rm RP} < 1$. The derivation of these estimates is given in Ref. 19.

Finally, $\delta_{\rm NP}$ must be small so that $T_{r\to y}$ is close to the ideal reference model T_0.

III. Optimization Problem Solved for Controller Synthesis

Consider the block diagram illustrated in Fig. 3. Let $\{\tilde M, \tilde N\}$ be a normalized LCF of the weighted plant G_s, T_0 the ideal reference

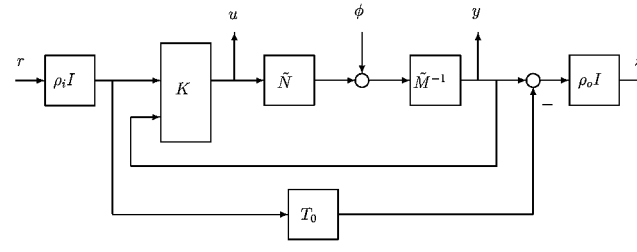

Fig. 3 Modified $\mathcal{H}_\infty$ loop shaping setup.

model, and ρ_i and ρ_o positive constants. A normalized left coprime factor uncertainty model is chosen ($T_{\phi \to [y \;\; u]^T}$) and the transfer matrix from r to z will be used to deduce information about the NP and RP with respect to T_0. The controller K can be partitioned as $K = [K_1 \;\; K_2]$.

The weighted plant G_s is assumed to have m inputs and p outputs, that is, $u \in \mathbb{R}^m$ and $r, y, z \in \mathbb{R}^p$. It is assumed that performance requirements are placed on all of the feedback signals; this does not have to be the case, it is done for notational convenience. Define

$$\Delta := \{\text{diag}(\Delta_1, \Delta_2) : \Delta_1 \in \mathbb{C}^{p \times p}, \Delta_2 \in \mathbb{C}^{p \times (p+m)}\}$$

$$\mathcal{M}(s) := \{\Delta(s) = \text{diag}(\Delta_{\text{perf}}, [\Delta_{\tilde{M}} \quad \Delta_{\tilde{N}}]) \in \mathcal{RL}_\infty : \Delta(s_0) \in \mathbf{\Delta}, \forall s_0 \in \bar{\mathbb{C}}_+\}$$

Let the transfer matrix from $[r \;\; \phi]^T \to [z \;\; y \;\; u]^T$ be denoted by M and partition M as

$$M = \left[\begin{array}{c|c} M_{11} & M_{12} \\ \hline M_{21} & M_{22} \end{array}\right]$$

where

$$M_{11} = \rho_o\left[(I - G_s K_2)^{-1} G_s K_1 - T_0\right]\rho_i$$

$$M_{12} = \rho_o (I - G_s K_2)^{-1} \tilde{M}^{-1}$$

$$M_{21} = \rho_i \begin{bmatrix} G_s \\ I \end{bmatrix} (I - K_2 G_s)^{-1} K_1$$

$$M_{22} = \begin{bmatrix} I \\ K_2 \end{bmatrix} (I - G_s K_2)^{-1} \tilde{M}^{-1}$$

Consider the following constrained minimization

$$\min_{\text{stab } K} \sup_{\omega \in \mathbb{R}} \mu_{\mathbf{\Delta}}[M(j\omega)] : \|M_{22}\|_\infty < \gamma_{\text{RS}} \tag{1}$$

Let

$$\Pi = \left\{\hat{G}_s = (\tilde{M} - \Delta_{\tilde{M}})^{-1}(\tilde{N} + \Delta_{\tilde{N}}) : [\Delta_{\tilde{M}} \quad \Delta_{\tilde{N}}] \in \mathcal{RL}_\infty\right\}$$

denote the set of perturbed weighted plant models. (The perturbed weighted plant models in Π also satisfy a winding number condition, see Theorem 1.20 of Ref. 14.) Assume that minimization (1) is solved and that $\sup_{\omega \in \mathbb{R}} \mu_{\mathbf{\Delta}}[M(j\omega)] < \gamma_{\text{RP}}$. It is obvious from the robust stability constraint that the closed-loop system will be stable for all $\hat{G}_s \in \Pi$ with

$$\|[\Delta_{\tilde{M}} \quad \Delta_{\tilde{N}}]\|_\infty \leq \gamma_{\text{RS}}^{-1}$$

The μ RP theorem (Theorem 11.9 of Ref. 20) guarantees that

$$\left\|(I - \hat{G}_s K_2)^{-1} \hat{G}_s K_1 - T_0\right\|_\infty < \delta_{\text{RP}} \tag{2}$$

where $\delta_{\text{RP}} = \gamma_{\text{RP}}/(\rho_i \rho_o)$, for all $\hat{G}_s \in \Pi$ with

$$\|[\Delta_{\tilde{M}} \quad \Delta_{\tilde{N}}]\|_\infty \leq \gamma_{\text{RP}}^{-1}$$

Equation (2) also guarantees an NP level of $\delta_{\text{NP}} = \delta_{\text{RP}}$, that is, the guaranteed RP and NP levels are equal. (This will be discussed further in Sec. VI.)

Therefore, minimization (1) can be used to synthesize controllers that come with the desired guarantees.

Define the set

$$\mathcal{D}_l := \{\text{diag}(dI_p, I_{p+m}) : d \in \mathbb{R}, d > 0\}$$

Every $D_l \in \mathcal{D}_l$ is associated with a $D_r = \text{diag}(d^{-1} I_p, I_p)$. It can be shown that for the $\mathbf{\Delta}$ under consideration (i.e., block diagonal with two blocks), at each frequency ω

$$\mu_{\mathbf{\Delta}}[M(j\omega)] = \inf_{D_l \in \mathcal{D}_l} \bar{\sigma}[D_l M(j\omega) D_r] \tag{3}$$

In general, Eq. (3) is an inequality ($\leq$) (see Sec. 11.2.3 of Ref. 20). Minimization (1) without the RS constraint is a standard μ-synthesis problem that has not yet been solved. A reasonable approach motivated by Eq. (3) is to solve

$$\min_{\text{stab } K} \inf_{D_l(s) \in \mathcal{D}_l(s)} \|D_l(s) M(s) D_r(s)\|_\infty \tag{4}$$

by iteratively solving for K and $D_l(s)$; this is the so-called D–K iteration. The set $\mathcal{D}_l(s)$ is defined as

$$\mathcal{D}_l(s) := \{D_l(s) = \text{diag}[d(s) I_p, I_{p+m}] : d(s), d^{-1}(s) \in \mathcal{RH}_\infty\}$$

Every $D_l(s) \in \mathcal{D}_l(s)$ is associated with a $D_r(s) = \text{diag}[d^{-1}(s) I_p, I_p]$ and $D_l(s)$ and $D_r(s)$ are chosen so that $D_r^{-1}(s)\Delta(s) = \Delta(s) D_l(s)$, where $\Delta(s) \in \mathcal{M}(s)$. For a fixed $D_l(s)$, $\min_K \|D_l(s) M(s) D_r(s)\|_\infty$ is a standard $\mathcal{H}_\infty$ optimization problem. For a given K, $\inf_{D_l(s) \in \mathcal{D}_l(s)} \|D_l(s) M(s) D_r(s)\|_\infty$ is a standard convex optimization problem that can be solved pointwise in the frequency domain,

$$\sup_{\omega \in \mathbb{R}} \inf_{D_l \in \mathcal{D}_l} \bar{\sigma}[D_l M(j\omega) D_r]$$

because, given the minimizing D_l across frequency, there is always a rational function $D_l(s) \in \mathcal{D}_l(s)$ whose gain approximates the D_l across frequency. The cost of Eq. (4) can be shown to decrease monotonically if the gain of $D_l(s)$ interpolates the D_l exactly, but there is no guarantee that a global minimum will be achieved. A μ-synthesis tutorial can be found in Ref. 21.

Similarly, because synthesis problem (1) has not yet been solved, a reasonable approach is to solve

$$\min_{\text{stab } K} \inf_{D_l(s) \in \mathcal{D}_l(s)} \|D_l(s) M(s) D_r(s)\|_\infty : \|M_{22}\|_\infty < \gamma_{\text{RS}} \tag{5}$$

using the D–K iteration. Because of the RS constraint, the K step of the D–K iteration is an infinite dimensional optimization problem. It is evident from Eq. (3) that for the $\mathbf{\Delta}$ under consideration the convex optimization problem mentioned corresponds to evaluating $\sup_{\omega \in \mathbb{R}} \mu_{\mathbf{\Delta}}[M(j\omega)]$. Hence, conservatism from the D step of the D–K iteration arises only from approximating the minimizing D_l across frequency.

IV. Solving the *K* Step of the Synthesis Problem

Minimization (5) is solved by iteratively solving for K and $D_l(s)$. To obtain K for a fixed $D_l(s)$ optimization problem

$$\min_{\text{stab } K} \|D_l(s) M(s) D_r(s)\|_\infty : \|M_{22}\|_\infty < \gamma_{\text{RS}} \tag{6}$$

will be approximated with a finite dimensional problem. Solving for $D_l(s)$ for a given K is done as discussed in the preceding section.

The finite dimensional problem is derived using the method proposed in Ref. 22, which deals with multiobjective output-feedback synthesis for multi-input/multi-output LTI systems. The approach in Ref. 22 is suboptimal because all of the closed-loop specifications are expressed by means of a single Lyapunov function; nevertheless, it has been found that the resulting synthesis technique works well in practice. Furthermore, it is numerically tractable because it leads to a linear matrix inequality (LMI) problem, which is readily solvable using commercial software.[23] In Ref. 19 it is shown that solving Eq. (6) amounts to solving an optimization problem with three LMIs and six matrix variables; the decision variables are typically of the order of the square of the number of states of $D_l(s) M(s) D_r(s)$.

V. Proposed Design Procedure

The designer uses a precompensator W_1, a postcompensator W_2, a constant $\rho = \sqrt{(\rho_o \rho_i)}$ (Fig. 3), and an ideal reference model T_0 to specify the control system requirements. The proposed design procedure is described hereafter:

1) Shape the singular values of G open loop with frequency-dependent weights W_1 and W_2 according to closed-loop objectives. This is done as in $\mathcal{H}_\infty$ loop shaping. Evaluate $\|T_{\phi \to [y \;\; u]^T}\|_\infty := \gamma_1$ (Fig. 3). The desired stability margin γ_{RS}^{-1} must obviously be $< \gamma_1^{-1}$. When designing the weights, care must be taken so that

the bandwidth of $N[\{M, N\}$ is a normalized right coprime factorization (RCF) of $G_s]$ is not smaller than the bandwidth of T_0 because this will lead to poor robust performance. Furthermore, $\max_i \delta_v(W_2\hat{G}_i W_1, W_2 G W_1) := \gamma_2$ should not be too large. ($\hat{G}_i$ are the perturbed plant models, see Sec. II.) The desired performance margin $\gamma_{\mathrm{RP}}^{-1}$ must be $> \gamma_2^{-1}$.

2) Design the ideal reference model T_0. In general, this is done using a performance-oriented control system design method. In the case of military aircraft, however, the MIL-STD can be used, see Sec. II.

3) Choose a sensible range for ρ and grid this range. At each point of the grid solve minimization (5) using the D–K iteration and the finite dimensional approximation of Eq. (6). Note that design examples indicate that two different pairs of (ρ_o, ρ_i) that have the same product lead to similar solutions. This is because of the structure of $\boldsymbol{\Delta}$ and depends on a) how well the gain of $D_l(s)$ interpolates the minimizing D_l and b) how well the finite dimensional problem presented in the preceding section approximates Eq. (6). (See the last comment of the next section.)

4) Plot δ_{RP} and $\gamma_{\mathrm{RP}}^{-1}$ against ρ. Both plots are monotonically decreasing. Pick the controller that guarantees the desired $\gamma_{\mathrm{RP}}^{-1}$.

5) Check time simulations and frequency responses of the resulting closed-loop system to verify that all of the controller specifications are satisfied. If the guaranteed value of δ_{RP} is too large, then, assuming that T_0 and γ_{RS} have been chosen sensibly, redesign the weights. (The estimates mentioned in Sec. II can be used to relate time-domain requirements to the RP level δ_{RP}.)

If a postcompensator W_2 is used, then guarantee (2) is not meaningful as such. Denote the perturbed plant model by $\hat{G}$. If it is assumed that no uncertainty is associated with W_2, then, at each frequency

$$\bar{\sigma}\left[(I - \hat{G}W_1K_2W_2)^{-1}\hat{G}W_1K_1W_2 - T_0\right]$$
$$\leq \bar{\sigma}\left(W_2^{-1}\right)\bar{\sigma}\left[(I - W_2\hat{G}W_1K_2)^{-1}W_2\hat{G}W_1K_1 - W_2T_0W_2^{-1}\right]\bar{\sigma}(W_2)$$

Because W_2 is typically used for noise rejection, it is usually a diagonal transfer matrix of low-pass filters. If T_0 is also chosen to be a diagonal transfer matrix, emphasising good output decoupling, then, from Eq. (2), it can be deduced that

$$\bar{\sigma}\left[(I - \hat{G}W_1K_2W_2)^{-1}\hat{G}W_1K_1W_2 - T_0\right] < \kappa(W_2)\delta_{\mathrm{RP}}$$

Because $\kappa(W_2)$ is commonly one at frequencies up to just above the bandwidth of T_0, the guaranteed robust performance level at these frequencies will be equal to δ_{RP}.

VI. Remarks on the Proposed Design Procedure

The setup illustrated in Fig. 3 was first considered in Ref. 3. The following optimization problem was proposed:

$$\min_{\text{stab } K} \left\| \left[\begin{array}{c|c} \rho^2\left[(I - G_sK_2)^{-1}G_sK_1 - T_0\right] & \rho(I - G_sK_2)^{-1}\tilde{M}^{-1} \\ \hline \rho G_s(I - K_2G_s)^{-1}K_1 & (I - G_sK_2)^{-1}\tilde{M}^{-1} \\ \rho(I - K_2G_s)^{-1}K_1 & K_2(I - G_sK_2)^{-1}\tilde{M}^{-1} \end{array}\right] \right\|_\infty \tag{7}$$

Minimization (7) does not always result in a control system with a satisfactory stability margin. As ρ increases, δ_{RP} decreases, but γ_{RP} increases, reducing the guaranteed stability margin. The structure of the problem is not exploited. Because $\mu_{\boldsymbol{\Delta}}[M(j\omega)]$ is bounded above by $\bar{\sigma}[M(j\omega)]$, minimization (7) will result in values of γ_{RP} greater than or equal to the values of γ_{RP} resulting from minimization (5), without the robust stability constraint.

An RP measure for the single DOF $\mathcal{H}_\infty$ loop shaping controller is derived in Theorem 4.6 of Ref. 14. Let G_s be the weighted plant and $\{M, N\}$ be a normalized RCF of G_s. If the $\mathcal{H}_\infty$ loop shaping controller has been implemented in the observer form, then the nominal transfer matrix from references to outputs is $T_{r\to y} = N$. (It is assumed that $W_2 = I$.) If the weighted plant is perturbed to $\hat{G}_s$, then the transfer matrix from references to outputs will be perturbed to $\hat{T}_{r\to y}$. The RP measure is given by

$$\|\hat{T}_{r\to y} - N\|_\infty \leq \alpha/\sin(\arcsin\epsilon - \arcsin\alpha)$$

$\forall \hat{G}_s : \delta_v(G_s, \hat{G}_s) \leq \alpha$, where $\epsilon = \gamma_{\mathrm{RS}}^{-1}$ is the achieved stability margin. Design experience has shown that $\alpha/\sin(\arcsin\epsilon - \arcsin\alpha)$ is larger than the values of δ_{RP} achieved when designing controllers using the method proposed in this paper for $\alpha = \gamma_{\mathrm{RP}}^{-1}$. Furthermore, N may not be close to the desired transfer matrix from references to outputs. The power of Vinnicombe's bound[14] is that it is a function of $\delta_v(G_s, \hat{G}_s)$.

The control system design specifications typically dictate that $T_{r\to y}(j0) = T_0(j0) = I$. This is not guaranteed by solving minimization (5); all that is guaranteed is that

$$\bar{\sigma}[T_{r\to y}(j0) - I] < \delta_{\mathrm{RP}}$$

Thus, a constant prefilter T_{dc} must be added to the control system so that at $\omega = 0$

$$T_{r\to y}T_{\mathrm{dc}} = (I - G_sK_2)^{-1}G_sK_1T_{\mathrm{dc}} = I$$

Unfortunately, T_{dc} will change the performance margin and the RP level. Let the modified transfer matrix from $[r\ \ \phi]^T \to [z\ \ y\ \ u]^T$ be denoted by M_{mod}. It can be deduced under some mild assumption (see Sec. 4.4 of Ref. 24) that

$$\hat{\gamma}_{\mathrm{RP}} := \mu_{\boldsymbol{\Delta}}[M_{\mathrm{mod}}(j\omega)] < \sqrt{\bar{\sigma}(T_{\mathrm{dc}})}\gamma_{\mathrm{RP}} + \gamma_{\mathrm{RS}}$$

where $\hat{\gamma}_{\mathrm{RP}}^{-1}$ is the modified performance margin. It can also be shown that

$$\bar{\sigma}(T_{\mathrm{dc}}) < 1/(1 - \delta_{\mathrm{RP}}) \Longrightarrow \hat{\gamma}_{\mathrm{RP}} < \left[\sqrt{1/(1 - \delta_{\mathrm{RP}})}\right]\gamma_{\mathrm{RP}} + \gamma_{\mathrm{RS}}$$

This upper bound has been found to be quite conservative. Nevertheless, it indicates that the smaller the value of δ_{RP}, the closer $\hat{\gamma}_{\mathrm{RP}}$ will be to γ_{RP}. It has been observed that T_{dc} produces better model matching at all frequencies because the optimization process tends to give $T_{r\to y}$ the same frequency response shape as T_0.

Intuition suggests that the need for a constant prefilter can be avoided by weighting r or z in Fig. 3 with a transfer matrix W, with W^{-1} being a high-pass filter. Unfortunately, this leads to poor values of $\gamma_{\mathrm{RP}}^{-1}$ because W also weights M_{12} or M_{21}. This scheme essentially optimizes nominal performance by optimizing robust performance at low frequency; something that is not desired.

It is clear that the cost of Eq. (5) is not guaranteed to be monotonically decreasing. [Minimization (5) is solved using the D–K iteration, and it is assumed that the gain of $D_l(s)$ fits the D_l data perfectly.] This is because the finite dimensional minimization that is used to approximate Eq. (6) optimizes over a subset of all stabilizing controllers. Nevertheless, the proposed design procedure works well in practice.

VII. HIRM Wind-Tunnel Model

The wind-tunnel model used for testing is geometrically similar to the HIRM originally used to investigate the feasibility of using nose suction as an actuator at high angles of attack.[25,26] The original HIRM is a control configured fighter aircraft with conventional control surfaces, tailplane, rudder, and canard, and new concept actuators, thrust vectoring, and nose suction. It has a length of 4.335 m and a semispan of 1.3 m. The wind-tunnel model, shown in Fig. 4, is scaled down by a factor of five. The size of the model is essentially limited by the wind-tunnel working section.

The rig (Fig. 4) is placed inside a $5\frac{1}{2} \times 4$ ft low-speed turbulent wind tunnel. The model aircraft has two DOF. It can yaw about the vertical rod. (The yaw angle is denoted by ψ.) It can also roll about an axis that coincides with its body x axis when $\psi = 0$ deg. (The roll angle is denoted by ϕ.) The model is set at a pitch angle θ_0 that remains fixed throughout each experiment.

There are two actuators for each DOF. The differential tailplane and thrusters at the top of the vertical rod provide rolling power, and the nose suction and air jets at the rear of the plane provide

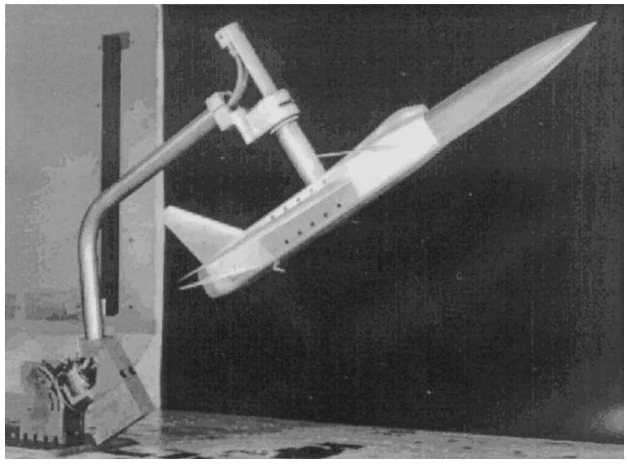

Fig. 4 Photograph of the rig.

yawing power. The required rolling moment could not be achieved by placing the roll jets inside the aircraft fuselage because the moment arm would be too small. The differential tailplane is actuated by a high-speed, high-torque model aircraft servo. The valves used to regulate the jets and suction have a very high bandwidth, and the attitude of the aircraft (ϕ and ψ) is measured by two high-resolution optical encoders. More details about the rig can be found in Ref. 10.

VIII. Controller Design and Flight Testing

Identified data were used to produce an LTI model of the rig about 30 deg of incidence, a wind-tunnel speed of 30 m/s, and wings level flight.[10] The LTI model of the rig, which is denoted by G_{id} and includes valve dynamics but no encoder dynamics, has two inputs, roll and yaw thrusters, and two outputs, roll ϕ and yaw ψ angle. The moments produced by the thrusters are measured in Newton meters and the angles are measured in radians. The identified model is given in the Appendix and has eight states and a real, unstable pole with a time constant of about 0.25 s.

An LTI controller is designed for the rig using the plant model G_{id} and the design procedure described in Sec. V. The feedback variables are the two measured angles ϕ and ψ. The performance specifications described in Sec. IV of Ref. 10 dictate that the desired closed-loop bandwidth of both channels is about 5 rad/s.

The precompensator is chosen to be

$$4\frac{s+3}{s}\frac{s+5}{0.02s+1}W_{\text{full}}$$

where

$$W_{\text{full}} = \frac{1}{s+0.979}\begin{bmatrix} 0.993s+1.635 & -0.002s+0.591 \\ -0.043s+0.867 & 1.030s+1.823 \end{bmatrix}$$

The nondiagonal weight W_{full} has been designed using the procedure proposed in Ref. 27 so that at low frequencies the minimum singular value of the weighted plant becomes approximately equal to its maximum singular value. No postcompensator is used, and the ideal reference model T_0 is chosen to be

$$T_0 = \frac{2^2}{s^2+2\times 0.8\times 2s+2^2}\frac{1}{0.02s+1}I_2$$

When T_0 is made diagonal, good output decoupling is emphasized. Time simulations will be carried out using perturbed plant models that result from changing the aerodynamic coefficients $\partial\ddot{\phi}/\partial\phi$ and $\partial\ddot{\psi}/\partial\psi$ of the nominal plant model by up to $\pm 100\%$. (Note that $\delta\ddot{\phi} = (\partial\ddot{\phi}/\partial\phi)\delta\phi + (\partial\ddot{\phi}/\partial\psi)\delta\psi + \cdots$.) The ν gap between every perturbed weighted plant and the nominal weighted plant is ≤ 0.15. The constraint $\gamma_{\text{RS}}^{-1} > 0.25$ is imposed on the stability margin. Note that constraints are also imposed on the size of two of the six matrix variables of the LMI problem solved to obtain the controller (the trace penalty in Table 1). The range chosen for ρ is the interval [2, 4]. This range is gridded, and minimization (5) is solved at each grid point. The result of the D–K iteration for $\rho = 3$ is given in Table 1. A constant prefilter is required. (The singular values of T_{dc} are 1.60 and 1.45.) The guaranteed $\delta_{\text{RP}} = 0.716$ and $\hat{\gamma}_{\text{RP}}^{-1} = 0.155$. The synthesized controller is model reduced from 27 to 15 states with no cost, and the implemented controller has 20 states.

Table 1 D–K iteration for $\rho = 3$

Iteration	γ_{RP}	γ_{RS}	$\hat{\gamma}_{\text{RP}}$	States of $D_l(s)$	Trace penalty
1	15.90	3.67	7.62	0	10^{-4}
2	6.53	3.69	7.61	2	10^{-4}
3	6.48	3.69	7.62	2	10^{-4}
4	5.94	3.81	7.40	2	10^{-6}
5	5.55	3.95	6.62	4	10^{-6}
6	6.05	3.98	6.61	4	10^{-8}
7	5.71	3.93	6.44	4	10^{-6}

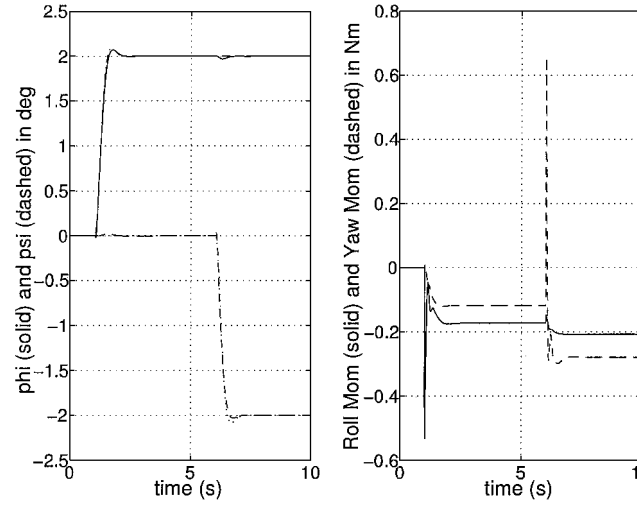

Fig. 5 Nominal response.

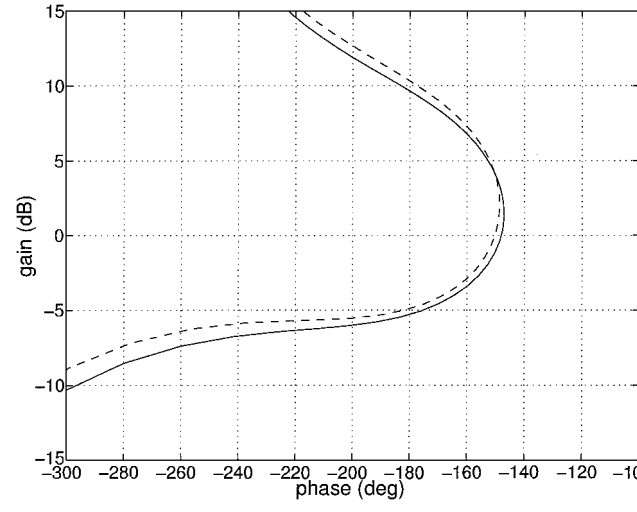

Fig. 6 Nichols plots for constrained (——) and unconstrained (- - -) case.

The time response of the nominal model G_{id} is illustrated in Fig. 5. The dash–dot and dashed lines in Fig. 5 are the ideal roll and yaw response. The demanded plant inputs can be obtained from Fig. 5 by multiplying the rolling and yawing moments by -1.

Figure 6 illustrates the Nichols plot of the transfer function that results from breaking the yaw loop at the plant input for both the constrained case [minimization (5) solved with $\gamma_{\text{RS}}^{-1} > 0.25$] and unconstrained case [minimization (5) solved with no constraint on γ_{RS}^{-1}]. When a constraint is imposed on the stability margin, the gain and phase margins have improved while maintaining good time-response properties. (Gain margin improves from -4.9 to -5.4 dB and phase margin from 29.7 to 32.0 deg.)

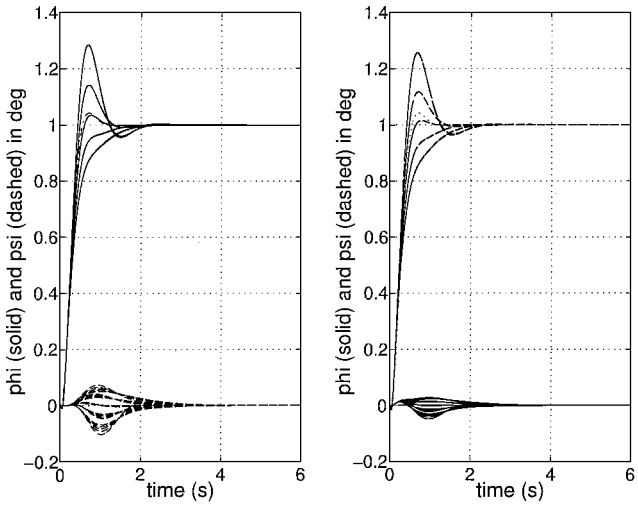

Fig. 7 Perturbed responses.

Figure 7 illustrates responses to step commands using the set of perturbed plant models described previously. As in Fig. 5, the dash-dot and dashed lines are the ideal roll and yaw response.

The controller tested in the wind tunnel is designed with the ideal reference model

$$T_0 = \frac{2^2}{s^2 + 2 \times 0.8 \times 2s + 2^2} \frac{1}{0.02s + 1} I_2$$

The bandwidth of T_0 has been reduced to ensure that the valves do not reach their position limits because of a large reference demand. The achieved $\gamma_{\mathrm{RS}}^{-1} = 0.254$. The guaranteed $\hat{\gamma}_{\mathrm{RP}}^{-1} = 0.185$, and $\delta_{\mathrm{RP}} = 0.600$. The implemented controller has 19 states.

The dSPACE GmbH software and hardware are used to control the wind-tunnel model. The processor used runs at 40 MHz (DS1003 digital signal processing board) and the 2-DOF controller was implemented at 100 Hz.

As can be seen in Figs. 8 and 9, the controller performs very well. The 2-DOF controller does not position or rate limit the thrusters, but uses them more than the 1-DOF controller flight tested in Ref. 10. The increased usage is probably because the weighted plant used for controller synthesis did not contain low-pass filters for noise rejection. Note that the large actuator usage drained the tank that supplied the compressed air and, as a result, closed-loop performance degraded, for example, see the overshoot in yaw angle in Fig. 9.

Our design procedure is conceptually and computationally more complex than standard 2-DOF $\mathcal{H}_\infty$ loop shaping, that is, the design procedure proposed in Ref. 3. Also, the synthesized controllers have more states than those obtained using standard 2-DOF $\mathcal{H}_\infty$ loop shaping (no model reduction), for example, in the case of the HIRM wind-tunnel model our 2-DOF control law has an extra eight states. However, if the control law specifications boil down to the three guarantees given in Sec. II, then our approach is more systematic. If the required disturbance rejection dynamics are much faster than the nominal tracking dynamics, then it may be possible to meet the control law specifications using $\mathcal{H}_\infty$ loop shaping or standard 2-DOF $\mathcal{H}_\infty$ loop shaping.

Once the designer becomes familiar with the metrics γ_{RS}, δ_{NP}, δ_{RP}, and γ_{RP} and how they relate to the control law specifications, then our design procedure is straightforward to use and not much more conceptually complex than standard 2-DOF $\mathcal{H}_\infty$ loop shaping. Computational complexity was not found to be an issue in the problems investigated; in the largest problem examined $D_l(s)M(s)D_r(s)$ had 31 states, that is, the resulting LMI problem had three LMIs and approximately 2200 decision variables. Note that LMI Lab[23] was used to solve the LMI problem and that the state-space data of $D_l(s)M(s)D_r(s)$ were scaled with a diagonal similarity transformation produced with the μ-tools command `sysc1`; larger problems may require more reliable solvers and better conditioning techniques. Because the additional controller states correspond to the states of the D scales that the designer sets directly, it is up to the designer to decide whether using additional states has a significant impact on the overall closed-loop performance.

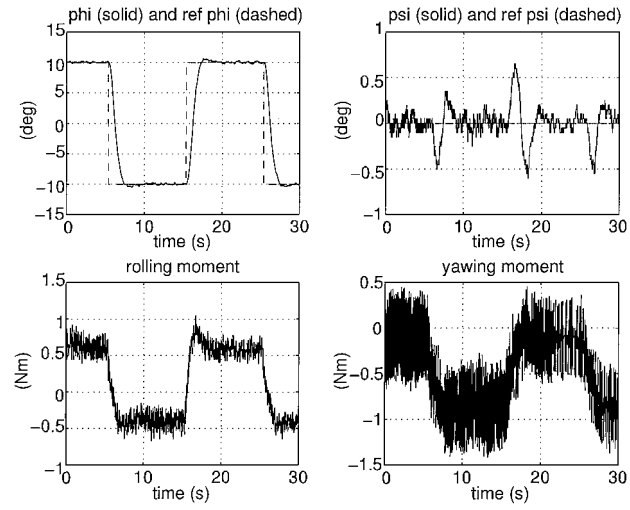

Fig. 8 Angle of $\phi_{\mathrm{dem}} = \pm 10$ deg and $\psi_{\mathrm{dem}} = 0$ deg.

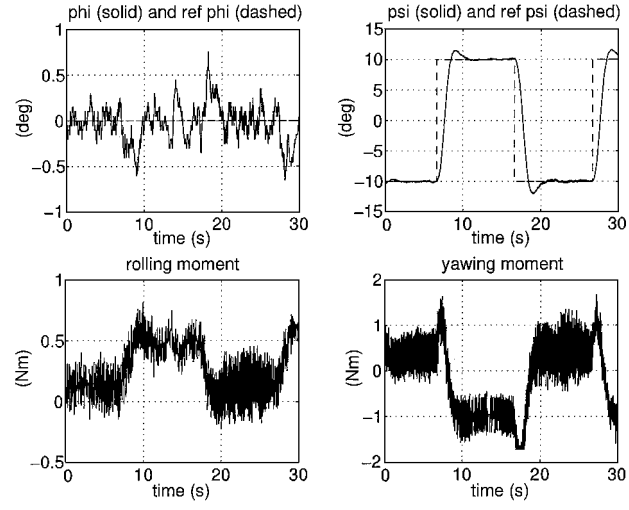

Fig. 9 Angle of $\psi_{\mathrm{dem}} = \pm 10$ deg and $\phi_{\mathrm{dem}} = 0$ deg.

IX. Conclusions

A robust 2-DOF controller has been designed for an actively controlled wind-tunnel model. The proposed design procedure uses the standard 2-DOF $\mathcal{H}_\infty$ loop shaping setup, but the optimization problem solved for controller synthesis is new: 1) The structure of the problem is exploited by using μ-synthesis techniques. 2) A robust stability constraint is included in the optimization. Exploiting the structure of the problem potentially leads to tighter closed-loop guarantees, and adding the RS constraint enables the designer to meet systematically additional control law specifications.

Controller synthesis is performed using a D–K iteration; the D step of the iteration is solved as in μ synthesis, and the K step, which is a constrained $\mathcal{H}_\infty$ norm minimization, is approximated with an LMI problem. For the examples considered, computational complexity associated with solving the LMI problem did not limit the practicality of our approach.

Conceptually, after becoming familiar with the metrics γ_{RS}, δ_{NP}, δ_{RP}, and γ_{RP}, our design procedure should become as straightforward to use as standard 2-DOF $\mathcal{H}_\infty$ loop shaping. Controller order is higher than in standard 2-DOF $\mathcal{H}_\infty$ loop shaping, but is controlled by the designer and is not critical in all applications.

The controller designed for the HIRM wind-tunnel model was flight tested and was found to perform very well.

Appendix: Identified Mod

The state-space matrices of the wind-tunnel model's rigid-body dynamics and the transfer function of each valve are

$$\left[\begin{array}{cccc|cc} 0 & 1 & 0 & 0 & 0 & 0 \\ -23.8 & -3.36 & 4.6 & -0.24 & 4.78 & 0 \\ 0 & 0 & 1 & 0 & 0 & 0 \\ -16.78 & -0.02 & 22.78 & -1.49 & 0 & 4.95 \\ \hline 1 & 0 & 0 & 0 & 0 & 0 \\ 0 & 0 & 1 & 0 & 0 & 0 \end{array}\right]$$

$$\frac{1}{0.01s+1}\,\frac{s-40}{s+40}$$

Acknowledgments

This work was done while George Papageorgiou was supported by the Bedford site of the Defense Evaluation and Research Agency, and the Engineering and Physical Sciences Research Council, United Kingdom. Revisions to this paper were supported under NASA Langley Research Center Cooperative Agreement NCC-1-337.

References

[1]Vidyasagar, M., *Control System Synthesis: A Coprime Factorization Approach*, MIT Press, Cambridge, MA, 1985, Chap. 6.7, pp. 219–227.

[2]Yaesh, I., and Shaked, U., "Two-Degree-of-Freedom $\mathcal{H}_\infty$-Optimization of Multivariable Feedback Systems," *IEEE Transactions on Automatic Control*, Vol. 36, No. 11, 1991, pp. 1272–1276.

[3]Limeber, D., Kasenally, E., and Perkins, J., "On the Design of Robust Two Degree of Freedom Controllers," *Automatica*, Vol. 29, No. 1, 1993, pp. 157–168.

[4]Giusto, A., and Paganini, F., "Robust Synthesis of Feedforward Compensators," *IEEE Transactions on Automatic Control*, Vol. 44, No. 8, 1999, pp. 1578–1582.

[5]Prempain, E., and Postlethwaite, I., "Feedforward Control: A Full-Information Approach," *Automatica*, Vol. 37, No. 1, 2001, pp. 17–28.

[6]Fialho, I., Balas, G., Packard, A., Renfrow, J., and Mullaney, C., "Gain-Scheduled Lateral Control of the F-14 Aircraft During Powered Approach Landing," *Journal of Guidance, Control, and Dynamics*, Vol. 23, No. 3, 2000, pp. 450–458.

[7]Walker, D., and Postlethwaite, I., "Advanced Helicopter Flight Control Using Two-Degree-of-Freedom $\mathcal{H}_\infty$ Optimization," *Journal of Guidance, Control, and Dynamics*, Vol. 19, No. 2, 1996, pp. 461–468.

[8]Smerlas, A., Postlethwaite, I., Walker, D., Strange, M., Howitt, J., Horton, R., Gubbels, A., and Baillie, S., "Design and Flight Testing of an $\mathcal{H}_\infty$ Controller for the NRC Bell 205 Experimental Fly-By-Wire Helicopter," AIAA Paper 98-4300, Aug. 1998.

[9]Iglesias, P., and Urban,T., "Loop Shaping Design for Missile Autopilots: Controller Configurations and Weighting Filter Selection," *Journal of Guidance, Control, and Dynamics*, Vol. 23, No. 3, 2000, pp. 516–525.

[10]Papageorgiou, G., and Glover, K., "Design, Development and Control of the HIRM Wind Tunnel Model," *Proceedings of the 38th IEEE Conference on Decision and Control*, Vol. 2, IEEE Publications, Piscataway, NJ, 1999, pp. 1529–1537.

[11]McFarlane, D., and Glover, K., "A Loop Shaping Design Procedure Using $\mathcal{H}_\infty$ Synthesis," *IEEE Transactions on Automatic Control*, Vol. 37, No. 6, 1992, pp. 759–769.

[12]Papageorgiou, G., and Glover, K., "$\mathcal{H}_\infty$ Loop Shaping: Why Is It a Sensible Procedure for Designing Robust Flight Controllers?" AIAA Paper 99-4272, July 1999.

[13]Doyle, J., Francis, B., and Tannenbaum, A., *Feedback Control Theory*, Macmillan, New York, 1992, Chaps. 7, 8, pp. 105–155.

[14]Vinnicombe, G., *Uncertainty and Feedback: $\mathcal{H}_\infty$ Loop-Shaping and the ν-Gap Metric*, Imperial College Press, London, 2001, pp. 40, 41, 104–166, 184, 185, 295, 296.

[15]Glover, K., Vinnicombe, G., and Papageorgiou, G., "Guaranteed Multi-Loop Stability Margins and the Gap Metric," *Proceedings of the 39th IEEE Conference on Decision and Control*, Vol. 4, IEEE Publications, Piscataway, NJ, 2000, pp. 4084, 4085.

[16]Hyde, R., *$\mathcal{H}_\infty$ Aerospace Control Design-A VSTOL Flight Application*, Advances in Industrial Control Series, Springer-Verlag, Berlin, 1995.

[17]Muir, E., *Robust Flight Control: A Design Challenge, GARTEUR*, Vol. 224 of Lecture Notes in Control and Information Sciences, Springer-Verlag, London, 1997, Chap. 27, pp. 419–443.

[18]Cantoni, M., and Vinnicombe, G., "Quantifying Uncertainty and Performance Using the ν-Gap Metric," AIAA Paper 99-4277, Aug. 1999.

[19]Papageorgiou, G., and Glover, K., "Design of a Robust Two-Degrees-of-Freedom Controller for an Actively Controlled Wind-Tunnel Model," AIAA Paper 99-4274, July 1999.

[20]Zhou, K., Doyle, J., and Glover, K., *Robust and Optimal Control*, 1st ed., Prentice–Hall, Upper Saddle River, NJ, 1996, pp. 281–283, 289.

[21]Balas, G., Doyle, J., Glover, K., Packard, A., and Smith, R., *μ-Analysis and Synthesis Toolbox User's Guide*, 2nd ed., MathWorks, Inc., Naticle, MA, 1995, pp. 7-75–7-130.

[22]Scherer, C., Gahinet, P., and Chilali, M., "Mutliobjective Output-Feedback Control via LMI Optimization," *IEEE Transactions on Automatic Control*, Vol. 42, No. 7, 1997, pp. 896–911.

[23]Gahinet, P., Nemirovski, A., Laub, A., and Chilali, M., *LMI Control Toolbox User's Guide*, 1st ed., Math Works, Inc., Naticle, MA, 1995, pp. 8-1–8-35.

[24]Papageorgiou, G., "Robust Control System Design: $\mathcal{H}_\infty$ Loop Shaping and Aerospace Applications," Ph.D. Dissertation, Dept. of Engineering, Univ. of Cambridge, Cambridge, England, U.K., July 1998.

[25]Ross, A. J., Jefferies, E., and Edwards, G., "Control of Forebody Vortices by Suction at the Nose of the RAE High Incidence Research Model," CP-494, AGARD, Paper 27, 1990.

[26]Ross, A. J., Jefferies, E., and Edwards, G., "Dynamic Wind Tunnel Tests on Control of Forebody Vortices with Suction," CP-497, AGARD, Paper 17, 1991.

[27]Papageorgiou, G., and Glover, K., "A Systematic Procedure for Designing Non-Diagonal Weights to Facilitate $\mathcal{H}_\infty$ Loop Shaping," *Proceedings of the 36th IEEE Conference on Decision and Control*, Vol. 3, IEEE Publications, Piscataway, NJ, 1997, pp. 2127–2132.